Ganglioside GM1 produces Aβ$_{40}$ cytotoxic protofibril structure

Manjeet Kumar[a], Magdalena I Ivanova[b] and Ayyalusamy Ramamoorthy[a*]

Monosialoganglioside GM1-bound amyloid β-peptides have been found in patients' brains exhibiting early pathological changes of Alzheimer's disease. Herein, we report the ability of free GM1 to modulate Aβ$_{40}$ aggregation resulting in the formation of short rod-like, cytotoxic Aβ$_{40}$ protofibrils with the ability to potentiate both Aβ$_{40}$ and Aβ$_{42}$ aggregation.

Alzheimer's disease (AD) is associated with the gradual accumulation of cross-β amyloid fibrils of Aβ$_{40}$ and Aβ$_{42}$ in brains. Protein and peptide fibrillation is not due to the direct conversion of soluble monomeric form to insoluble amyloid fibrils. Instead, multiple intermediate processes may be involved, including the formation of prefibrillar or protofibrillar species that mainly act as primary or secondary nuclei for further fibril growth.[1] These intermediate aggregates are considered to be the dominant cytotoxic forms of misfolded proteins/ peptides.[2–4]

Yanagisawa et al. identified a unique GM1 ganglioside-bound Aβ species in the brains of patients with early pathological changes associated with AD.[5,6] Gangliosides, including GM1, are abundantly found in the neuronal membrane. Generally, free gangliosides are released in the extracellular region from the damaged cell membrane.[7,8] Several studies have demonstrated that ganglioside clusters in the membrane catalyze the formation of toxic Aβ species.[9–17] Additionally, free lipids have been shown to modulate the aggregation kinetics of Aβ peptides.[18–21] This *in vitro* study is focused on unraveling the molecular processes underlying the early conformational changes of Aβ induced by the interaction with GM1, which have been linked to early AD onset. Our results show that Aβ$_{40}$ produced Thioflavin T (ThT)-positive, cytotoxic, rod-like structures of varying sizes in the presence of GM1. Ganglioside induced Aβ$_{40}$ species were able to catalyze the conversion of unfolded monomeric Aβ$_{40}$ and Aβ$_{42}$ to β-sheet rich structures.

The interaction of Aβ$_{40}$ with GM1 was monitored via ThT fluorescence assay (Fig.1A). *In vitro* experiments, carried out at physiologically relevant pH and temperature conditions, reported the formation of Aβ$_{40}$ aggregates via a nucleation-dependent polymerization, typically displaying a sigmoidal curve with a prominent lag-phase, a growth phase, and an equilibrium phase.[22,23] Our Aβ$_{40}$ samples showed similar aggregation kinetics with a lag-phase (T_{lag}) of around 8.8 hours (h). T_{lag} for the formation of β-sheet rich species in Aβ$_{40}$ alone and GM1-containing samples were deduced from the ThT fluorescence data fitted to a sigmoidal function (Fig.1A).[24] Interestingly, there was a significant reduction in the lag-phase of Aβ$_{40}$ amyloid fibril formation and a slight increase in ThT fluorescence upon the addition of increasing concentration of GM1. A 1 μM GM1 was sufficient to reduce the lag-phase of 10

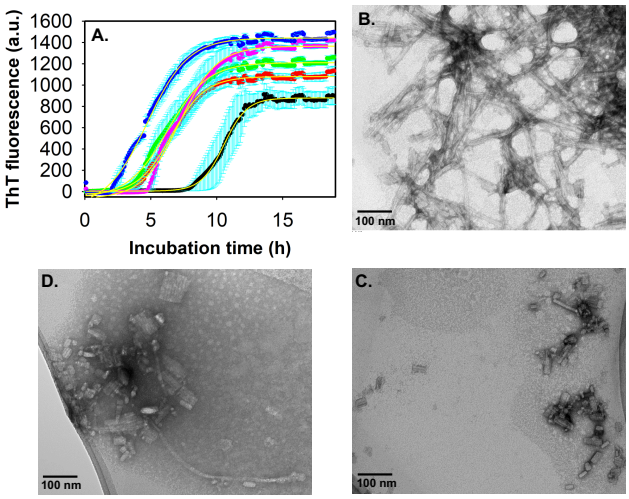

Figure 1. Probing the interaction between Aβ40 and GM1. (A) ThT fluorescence intensity of 10 μM Aβ40 (black) and varying concentrations of GM1: 1 μM (red), 2.5 μM (green), 20 μM (magenta) and 40 μM (blue) in 20 mM phosphate buffer, pH 7.4 at 37° C, slow continuous shaking. The line of best fit (yellow) through the data points was obtained by global fitting the data with a sigmoidal function.[24] TEM images of 10 μM Aβ40 alone (B), and in the presence of 1 μM GM1 (C, D), acquired after 48 h incubation at physiological pH and temperature conditions. Scale bars, as indicated. All other details on the sample preparation, experimental conditions, data processing, and instrument are given in the supporting information.

[a.] *Biophysics, Department of Chemistry, Biomedical Engineering, Macromolecular Science and Engineering, Michigan Neuroscience Institute, University of Michigan, Ann Arbor, MI 48109-1055, USA. E-mail: ramamoor@umich.edu.*
[b.] *Department of Neurology, University of Michigan, Ann Arbor, MI 48109*

†Electronic Supplementary Information (ESI) available: [details of any supplementary information available should be included here].

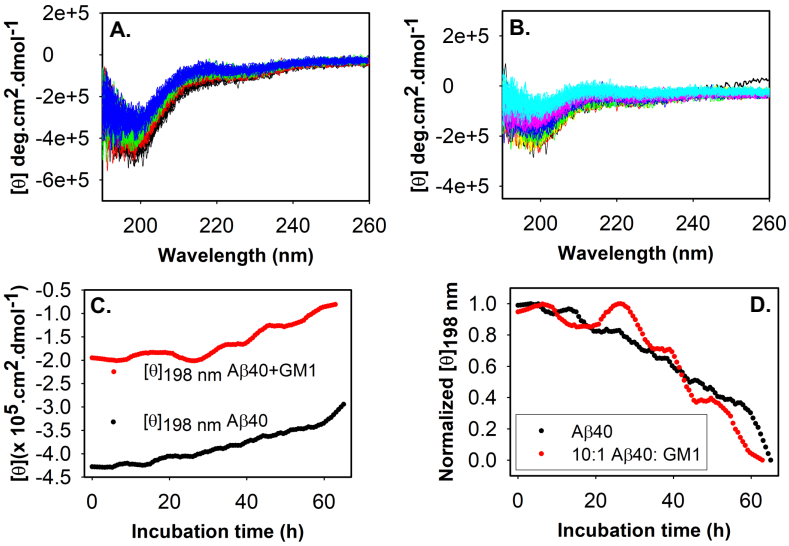

Figure 2. Comparing the rate of Aβ40's secondary structure change during fibrillation in the absence and presence of GM1 via far-UV CD. Molar ellipticity over the period of approximately 65 h of 20 μM Aβ40 (A): black (~ 0 – 15 h), red (~ 15 – 35 h), green (~ 35 – 45 h), blue (~ 45 – 65 h). Spectra of 20 μM Aβ40 + 2 μM GM1 (B): black (~ 0 – 1h), red (~ 1 – 4 h), yellow (~ 4 – 18 h), blue (~ 18 – 30 h), magenta (~ 30 – 43 h), cyan (~ 43 – 63 h). Samples were prepared in 20 mM phosphate buffer, pH 7.4 at 37° C. Spectrum acquisition time was 4 min. (C) Molar ellipticity of 20 μM Aβ40 (black) and 20 μM Aβ40 + 2 μM GM1 (red) at 198 nm over a period of ~ 63 h. (D) Normalized molar ellipticity at 198 nm of Aβ40 in the absence and presence of GM1 as indicated. All other details are provided in the supplementary information.

μM $A\beta_{40}$ by 4.8 h. The decrease in the lag-phase and the increase in ThT fluorescence intensity suggested an acceleration of $A\beta_{40}$ fibril formation. To confirm the above observation, TEM images were acquired from 10 μM $A\beta_{40}$ after incubation for 48 hours at physiological pH and temperature in the absence (Fig.1B) and the presence of 1 μM GM1 (Fig.1C, Fig.1D). $A\beta_{40}$ alone showed the presence of typical long amyloid fibril as previously reported.[25] However, the significantly shorter rod-like fibrillar structure of varying length and width was observed in GM1 modulated $A\beta_{40}$. Among heterogeneous population of dominant short, rod-like GM1-modified $A\beta_{40}$ species, a rare long fibril, most likely of non-GM1 bound $A\beta_{40}$ was also observed. The rod-like $A\beta_{40}$ filaments bind more efficiently to ThT, indicating they have similar cross-β architecture as observed in most amyloid fibrils.[26,27]

Several studies have suggested ganglioside nanoclusters in neuronal membranes induce a conformational change in $A\beta_{40}$.[28–30] So, we were interested in examining if the $A\beta_{40}$ can also undergo a secondary structure transition in the presence of GM1. Far-UV circular dichroism (CD) of 20 μM $A\beta_{40}$ in the absence and presence of 2 μM GM1, monitored over 62 h at physiological pH and temperature, did not show any change except for the decrease in random-coil content, as evidenced by the reduction of negative ellipticity peak at 198 nm (Fig.2C). An immediate decrease in random-coil content in $A\beta_{40}$ with no subsequent appearance of other secondary structure peaks as soon as GM1 was added suggest a fraction of $A\beta_{40}$ rapidly forms insoluble aggregates/nuclei. This may explain the reduction in the lag-phase of GM1-containing $A\beta_{40}$ in Figure 1. After that, we compared the molar ellipticity of $A\beta_{40}$ with GM1 at 198 nm to the $A\beta_{40}$ alone sample (Fig.2C, Fig.2D). Both $A\beta_{40}$ samples displayed a similar rate of change in the random coil during their aggregation. Overall, we infer that the nucleating species forming the β-sheet-rich structure are similar in both samples. Moreover, the apparent rate constant (k_{app}) for the formation of β-sheet rich species in $A\beta_{40}$ alone and GM1-containing samples were deduced from the ThT fluorescence data fitted to a sigmoidal function (Fig.1A).[24] The k_{app} for 10 μM $A\beta_{40}$ alone is 0.019/h, while the k_{app} for 10 μM $A\beta_{40}$ in the presence of 1 μM, 2.5 μM, 20 μM, and 40 μM are 0.013/h, 0.011/h, 0.012/h and 0.01/h, respectively. The comparatively similar k_{app} for GM1-containing $A\beta_{40}$ and the absence of long fibrillar species (Fig.1C) compared to $A\beta_{40}$ alone suggested that GM1 inhibited the elongation of $A\beta_{40}$ fibrils.

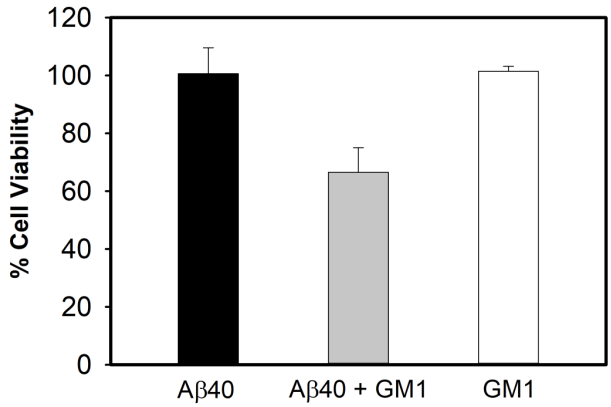

Figure 3. Evaluation of GM1-induced Aβ40 protofibril cytotoxicity. The MTT assay was used to measure differentiated human neuroblastoma SH-SY5Y cellular metabolic activity as an indicator of cell viability upon treatment with solutions containing 10 μM Aβ40 species without (black) and with (grey) 1 μM GM1 after 2 days of incubation. The white bar is of 2-day old 1 μM GM1 alone. See the supporting information for additional details.

The ThT, TEM imaging, and far-UV CD data confirm that the short rod-like $A\beta_{40}$ species generated upon interaction with GM1 is an on-pathway stable intermediate, most likely protofibrils of fully matured fibrils of $A\beta_{40}$. Interestingly, metastable protofibril of Aβ with the ability to alter the electrical activity of neurons, causing neuronal loss, has been reported earlier.[31–33] We, therefore, performed a cell viability assay on differentiated human neuroblastoma SH-SY5Y cells treated with samples containing $A\beta_{40}$ fibril, GM1-modulated $A\beta_{40}$ protofibril, and GM1 alone (Fig.3). Sample containing 10 μM $A\beta_{40}$ fibril alone did not show any significant cell cytotoxicity on differentiated SH-SY5Y cells, as reported earlier.[34] However,

we observed approximately 34% less cellular metabolic activity from differentiated SH-SY5Y cells upon incubation with GM1-induced $A\beta_{40}$ protofibrils. A 2 µM GM1 (alone) incubated for 48 h showed no cell death. This observation implies that $A\beta_{40}$ protofibrils are potentially cytotoxic.

Apart from the direct toxic effect displayed by the intermediates of many amyloid-forming proteins, as observed in this study, aggregating proteins can additionally catalyze the conversion of other amyloid or neighbouring proteins/peptides to aggregates[35]. The formation of amyloid fibrils from normal functional, misfolded, or unfolded proteins mostly follows nucleation-dependent polymerization similar to

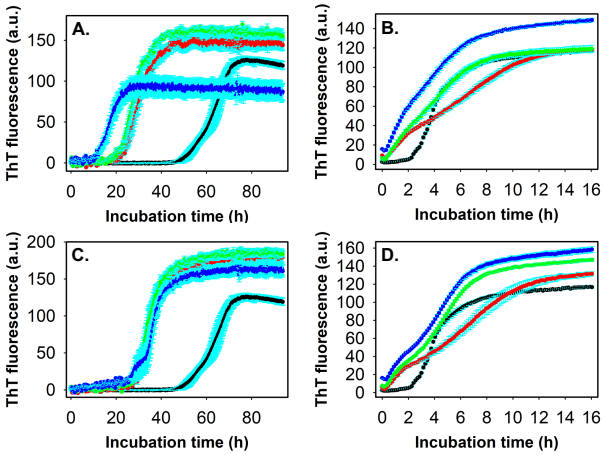

Figure 4. Seeding and cross-seeding of Aβ40 and Aβ42 with pre-formed Aβ40 aggregates. (A) ThT fluorescence profiles of 5 µM Aβ40 alone (black) and in the presence of 1% v/v (red), 2.5% v/v (green) and 5% v/v (blue) pre-formed Aβ40 amyloid fibril in 20 mM phosphate buffer, pH 7.4, 37° C under quiescent condition. (B) ThT fluorescence profiles of 5 µM Aβ42 alone (black) and in the presence of 1% v/v (red), 2.5% v/v (green) and 5% v/v (blue) pre-formed Aβ40 amyloid fibril in 20 mM phosphate buffer, pH 7.4, 37° C under quiescent condition. (C) ThT fluorescence profiles of 5 µM Aβ40 alone (black circle) and in the presence of 1% v/v (red circle), 2.5% v/v (green circle) and 5% v/v (blue circle) pre-formed GM1-induced Aβ40 protofibril in aforementioned conditions. (D) ThT fluorescence profiles of 5 µM Aβ42 alone (black circle) and in the presence of 1% v/v (red circle), 2.5% v/v (green circle) and 5% v/v (blue circle) pre-formed GM1-induced Aβ40 protofibril in above mentioned conditions. Appropriate blank was subtracted in each case. See the supporting information for additional details.

crystallization.[36,37] The critical step in these processes is the generation of the smallest unit, often termed nuclei (seeds), that can promote the formation of amyloids by rapidly converting non-aggregated proteins/peptides into fibrils.[32] There are two types of polymerization: homogenous polymerization, where both the nuclei and precursor proteins/peptides are the same, and heterogeneous polymerization (cross-seeded), in which the nuclei of one protein/peptide seed the aggregation of a different protein/peptide. Apart from primary nucleation, secondary nucleation, which is generally surface-catalyzed conversion of proteins/peptides to amyloid fibrils, can also lead to fibril proliferation[38]. The rapid transformation of non-aggregated proteins/peptides through primary and secondary nucleation has been established as a central process explaining the "infectious" nature of prion proteins in prion diseases, and the spread of pathogenic inclusions in many neurodegenerative disorders, including AD.[39–41] Knowing the importance of nucleation in AD, we studied whether GM1-induced $A\beta_{40}$ protofibril can catalyze the conversion of $A\beta_{40}$ and $A\beta_{42}$ (second major isomer generated from amyloid precursor protein involved in AD pathogenesis) to β-sheet rich structure. Using the ThT fluorescence assay we studied the secondary nucleation process of $A\beta_{40}$ by adding varying amounts of preformed $A\beta_{40}$ fibril to 5 µM of monomeric $A\beta_{40}$ under the quiescent condition at physiological pH and temperature (Fig.4A). Addition of 1%, 2.5% and 5% v/v preformed fibril as seed, significantly reduced the lag-phase of 5 µM $A\beta_{40}$ aggregation kinetics. Meanwhile, additions of 1%, 2.5%, and 5% v/v preformed $A\beta_{40}$ fibril to 5 µM of monomeric $A\beta_{42}$ led to a spontaneous increase in ThT fluorescence, suggesting immediate $A\beta_{42}$ fibril formation (Fig.4B). Seeding and cross-seeding of $A\beta_{40}$ and $A\beta_{42}$ respectively has earlier been observed with sonicated $A\beta_{40}$ fibril.[42] However, in our study, we used unsonicated $A\beta_{40}$ fibril as seeds. Similar to the secondary nucleation observed with $A\beta_{40}$ fibril, GM1-induced $A\beta_{40}$ protofibril also catalyzed the aggregation of monomeric $A\beta_{40}$ and $A\beta_{42}$.

As summarized in supplementary figure 1, we have shown the formation of short rod-like intermediate of $A\beta_{40}$, particularly stable protofibril structure upon interaction with ganglioside GM1. The GM1-induced $A\beta_{40}$ protofibril reduced the viability of human neuroblastoma cells, SHSY5Y. Potential implications of novel $A\beta_{40}$ species reported in this study include: GM1-bound $A\beta_{40}$ may be secreted into the extracellular space and act as a "seed" for other amyloid-forming proteins/peptides, leading to a large-scale aggregation.[43,44] Thus, our findings may explain the molecular basis for the early pathological changes observed in some patients with AD. In hindsight, the generation of stable, neurotoxic, protofibrillar assemblies of $A\beta_{40}$ exhibiting prion-like properties to seed the aggregation of other proteins could contribute more to the neurodegeneration than the other observed oligomeric and amyloid fibrils. From a therapeutic perspective, blocking the formation of intermediates resembling those described here could be a successful strategy in combating neurodegenerative diseases, including AD.

Authors Contributions:

M.K. and A.R. designed the research; M.K. performed the experiments and processed the data; M.K., M.I. and A.R. analyzed the data; M.K., M.I. and A.R. wrote the manuscript; A.R. directed the project.

Conflicts of interest

There are no conflicts to declare.

Acknowledgment

This study was supported by the National Institutes of Health Grants (AG048934 and DK13221401 to A.R.).

Notes and references

1 F. Chiti and C. M. Dobson, *Annu Rev Biochem*, 2006, **75**, 333–366.
2 J. Hardy and D. J. Selkoe, *Science*, 2002, **297**, 353–356.
3 C. C. Glabe, *Subcell Biochem*, 2005, **38**, 167–177.

Please do not adjust margins

4 P. H. Nguyen, A. Ramamoorthy, B. R. Sahoo, J. Zheng, P. Faller, J. E. Straub, L. Dominguez, J. E. Shea, N. v. Dokholyan, A. de Simone, B. Ma, R. Nussinov, S. Najafi, S. T. Ngo, A. Loquet, M. Chiricotto, P. Ganguly, J. McCarty, M. S. Li, C. Hall, Y. Wang, Y. Miller, S. Melchionna, B. Habenstein, S. Timr, J. Chen, B. Hnath, B. Strodel, R. Kayed, S. Lesné, G. Wei, F. Sterpone, A. J. Doig and P. Derreumaux, *Chem Rev*, 2021, **121**, 2545–2647.

5 K. Yanagisawa, A. Odaka, N. Suzuki and Y. Ihara, *Nat Med*, 1995, **1**, 1062–1066.

6 K. Yanagisawa and Y. Ihara, *Neurobiol Aging*, 1998, **19**, S65–S67.

7 P. S. Sastry, *Prog Lipid Res*, 1985, **24**, 69–176.

8 P. Davidsson, A. Wallin, P. Fredman, C. G. Gottfries, I. Karlsson, J. E. Månsson, L. Svennerholm and K. Blennow, *Arch Neurol*, 1991, **48**, 1032–1035.

9 K. Matsuzaki, *Biochim Biophys Acta Biomembr*, , DOI:10.1016/J.BBAMEM.2020.183233.

10 S. Fukunaga, H. Ueno, T. Yamaguchi, Y. Yano, M. Hoshino and K. Matsuzaki, *Biochemistry*, 2012, **51**, 8125–8131.

11 T. Okada, K. Ikeda, M. Wakabayashi, M. Ogawa and K. Matsuzaki, *J Mol Biol*, 2008, **382**, 1066–1074.

12 M. Ogawa, M. Tsukuda, T. Yamaguchi, K. Ikeda, T. Okada, Y. Yano, M. Hoshino and K. Matsuzaki, *J Neurochem*, 2011, **116**, 851–857.

13 T. Okada, M. Wakabayashi, K. Ikeda and K. Matsuzaki, *J Mol Biol*, 2007, **371**, 481–489.

14 J. Saha, P. Bose, S. Dhakal, P. Ghosh and V. Rangachari, *Biochemistry*, 2022, **61**, 2206–2220.

15 K. Matsuzaki, K. Kato and K. Yanagisawa, *Prog Mol Biol Transl Sci*, 2018, **156**, 413–434.

16 K. Matsuzaki, K. Kato and K. Yanagisawa, *Biochim Biophys Acta*, 2010, **1801**, 868–877.

17 A. Kakio, S. ichi Nishimoto, K. Yanagisawa, Y. Kozutsumi and K. Matsuzaki, *Biochemistry*, 2002, **41**, 7385–7390.

18 A. Chakravorty, S. D. McCalpin, B. R. Sahoo, A. Ramamoorthy and C. L. Brooks, *J Phys Chem Lett*, 2022, **13**, 9303–9308.

19 K. J. Korshavn, C. Satriano, Y. Lin, R. Zhang, M. Dulchavsky, A. Bhunia, M. I. Ivanova, Y. H. Lee, C. la Rosa, M. H. Lim and A. Ramamoorthy, *J Biol Chem*, 2017, **292**, 4638–4650.

20 K. Dahse, M. Garvey, M. Kovermann, A. Vogel, J. Balbach, M. Fändrich and A. Fahr, *J Mol Biol*, 2010, **403**, 643–659.

21 M. F. Sciacca, F. Lolicato, C. Tempra, F. Scollo, B. R. Sahoo, M. D. Watson, S. García-Viñuales, D. Milardi, A. Raudino, J. C. Lee, A. Ramamoorthy and C. la Rosa, *ACS Chem Neurosci*, 2020, **11**, 4336–4350.

22 G. Meisl, J. B. Kirkegaard, P. Arosio, T. C. T. Michaels, M. Vendruscolo, C. M. Dobson, S. Linse and T. P. J. Knowles, *Nature Protocols 2016 11:2*, 2016, **11**, 252–272.

23 B. R. Sahoo, S. J. Cox and A. Ramamoorthy, *Chem Commun (Camb)*, 2020, **56**, 4627.

24 A. M. Morris, M. A. Watzky and R. G. Finke, *Biochimica et Biophysica Acta (BBA) - Proteins and Proteomics*, 2009, **1794**, 375–397.

25 J. Wang, T. Yamamoto, J. Bai, S. J. Cox, K. J. Korshavn, M. Monette and A. Ramamoorthy, *Chemical Communications*, 2018, **54**, 2000–2003.

26 R. Khurana, C. Coleman, C. Ionescu-Zanetti, S. A. Carter, V. Krishna, R. K. Grover, R. Roy and S. Singh, *J Struct Biol*, 2005, **151**, 229–238.

27 M. Biancalana and S. Koide, *Biochim Biophys Acta Proteins Proteom*, 2010, **1804**, 1405–1412.

28 T. Okada, M. Wakabayashi, K. Ikeda and K. Matsuzaki, *J Mol Biol*, 2007, **371**, 481–489.

29 T. Matsubara, H. Yasumori, K. Ito, T. Shimoaka, T. Hasegawa and T. Sato, *Journal of Biological Chemistry*, 2018, **293**, 14146–14154.

30 T. Matsubara, M. Nishihara, H. Yasumori, M. Nakai, K. Yanagisawa and T. Sato, *Langmuir*, 2017, **33**, 13874–13881.

31 D. M. Hartley, D. M. Walsh, C. P. Ye, T. Diehl, S. Vasquez, P. M. Vassilev, D. B. Teplow and D. J. Selkoe, *J Neurosci*, 1999, **19**, 8876–8884.

32 D. M. Walsh, A. Lomakin, G. B. Benedek, M. M. Condron and D. B. Teplow, *Journal of Biological Chemistry*, 1997, **272**, 22364–22372.

33 J. D. Harper, S. S. Wong, C. M. Lieber and P. T. Lansbury, *Biochemistry*, 1999, **38**, 8972–8980.

34 J. Krishtal, O. Bragina, K. Metsla, P. Palumaa and V. Tõugu, *PLoS One*, , DOI:10.1371/JOURNAL.PONE.0186636.

35 M. I. Ivanova, Y. Lin, Y. H. Lee, J. Zheng and A. Ramamoorthy, *Biophys Chem*, , DOI:10.1016/J.BPC.2020.106507.

36 E. Chatani and N. Yamamoto, *Biophys Rev*, 2018, **10**, 527–534.

37 J. T. Jarrett and P. T. Lansbury, *Cell*, 1993, **73**, 1055–1058.

38 M. Törnquist, T. C. T. Michaels, K. Sanagavarapu, X. Yang, G. Meisl, S. I. A. Cohen, T. P. J. Knowles and S. Linse, *Chemical Communications*, 2018, **54**, 8667–8684.

39 L. C. Walker, J. Schelle and M. Jucker, *Cold Spring Harb Perspect Med*, , DOI:10.1101/CSHPERSPECT.A024398.

40 S. B. Prusiner, *Science*, 2012, **336**, 1511–1513.

41 P. Arosio, T. P. J. Knowles and S. Linse, *Physical Chemistry Chemical Physics*, 2015, **17**, 7606.

42 J. Tran, D. Chang, F. Hsu, H. Wang and Z. Guo, *FEBS Lett*, 2017, **591**, 177.

43 K. Yanagisawa, A. Asami-Odaka, N. Suzuki and Y. Ihara, *Ann N Y Acad Sci*, 1996, **786**, 184–194.

44 H. Hayashi, N. Kimura, H. Yamaguchi, K. Hasegawa, T. Yokoseki, M. Shibata, N. Yamamoto, M. Michikawa, Y. Yoshikawa, K. Terao, K. Matsuzaki, C. A. Lemere, D. J. Selkoe, H. Naiki and K. Yanagisawa, *Journal of Neuroscience*, 2004, **24**, 4894–4902.